Functional communication between endogenous BRCA1 and its partner, BARD1, during *Xenopus laevis* development

Vladimir Joukov, Junjie Chen*, Edward A. Fox, Jeremy B. A. Green†, and David M. Livingston†‡

Dana–Farber Cancer Institute and Harvard Medical School, 44 Binney Street, Boston, MA 02115

Contributed by David M. Livingston, August 14, 2001

The breast and ovarian susceptibility protein 1 (BRCA1) heterodimerizes with its structural relative, the BRCA1-associated RING domain protein (BARD1), which may have tumor suppressing function in its own right. Both proteins have evolved from a common evolutionary ancestor, and both exist in *Xenopus laevis* where, similar to their mammalian homologs, they form functional heterodimers. Depleting frog embryos of either BARD1 or BRCA1 led to similar and widely defective developmental phenotypes as well as depletion of the other polypeptide due to its decreased stability. Thus, each protein, in part, controls the abundance, stability, and function of the other, and these effects are heterodimerization-dependent. The interdependent nature of BRCA1 and BARD1 function supports the view that BARD1/BRCA1 heterodimers play a major role in breast and ovarian cancer suppression.

Mammalian BRCA1-associated RING domain protein (BARD1) and its heterodimerizing partner, breast and ovarian cancer susceptibility protein 1 (BRCA1), share limited sequence homology with other known proteins, although both contain an N-terminal RING finger domain and paired C-terminal BRCT motifs (1, 2). BARD1 also contains three tandemly repeated, centrally located ankyrin motifs (2).

BRCA1 null mice undergo early embryonic arrest—i.e., with embryos demonstrating severe cellular proliferation and gastrulation defects (3–5). Thus, *BRCA1* is likely a multifunctional, embryonic survival gene.

Cells of BRCA1-deficient mice readily develop a variety of chromosomal abnormalities, an indication of a role for BRCA1 in the maintenance of the genome integrity (6, 7). In this regard, BRCA1 interacts with multiple proteins involved in DNA recombination and repair, including Rad51, Mre11/Rad50/NBS1, BRCA2, Bloom's helicase, and a recently discovered DEAH helicase, BACH1 (8–12). Indeed, it plays a major role in sustaining normal double-strand (ds) break repair and homologous recombination, as well as transcription-coupled repair (13–16). There is a strong correlation between its role in genome integrity control and its tumor suppression function, suggesting that these two functions are linked.

Knowledge of BARD1 function is more limited. Suppression of its expression in a mouse mammary epithelial cell line induced biological changes, suggestive of a premalignant phenotype (17). Moreover, BARD1 is suspected of having tumor suppression function, with disease-specific effects in the breast, ovary, and uterus (18). In that guise, BARD1/BRCA1 complex formation could be viewed as an interaction of equals, both dedicated to the suppression of female-specific malignancies. How these effects are generated is a mystery.

BARD1 also interacts with and inhibits the polyadenylation factor, CstF-50, thereby participating in events that connect DNA damage to RNA processing control (19, 20). Moreover, the BRCA1 RING domain must be intact for BARD1 binding, for BRCA1-dependent double-strand break repair, and for BRCA1 tumor suppression function (2, 15). How these activities interconnect with one another is unclear, but BARD1/BRCA1 heterodimer formation likely constitutes part of the story.

In addition, the BRCA1 and BARD1 RING domains each possess *in vitro* E3 ubiquitin autoligase activity, which increased dramatically following heterodimer formation (21–23). This *in vitro* activity is, at a minimum, a reflection of the normal conformation of the BRCA1 N-terminal region (23). The *in vivo* significance of the heterodimeric E3 function has been unclear.

Here we report the identification, isolation, and functional characterization of *Xenopus laevis* BRCA1 and BARD1. These proteins are structural and functional homologs of their mammalian equivalents, and the dynamic nature of their *in vivo* behavior sheds light on why at least some of their functions are interrelated.

Materials and Methods

Isolation and Subcloning of *X. laevis BRCA1* and *BARD1* cDNAs and mRNA Production. *Xenopus BRCA1* and *BARD1* 3′ cDNA fragments were isolated by reverse transcription (RT)-PCR using degenerate primers, cloned, and then used to screen a stage-18 *Xenopus* cDNA library for full-length products (see supporting *Methods*, which are published as supporting information on the PNAS web site, www.pnas.org). Full-length *xBRCA1* and *xBARD1* cDNAs were subcloned into pCS2+ (24). To prevent their annealing to antisense morpholino oligonucleotides (MOs), the 5′ noncoding portions of these cDNAs were deleted and substituted with predesigned sequences by a PCR-based cloning technique (see supporting *Methods*).

The proteins encoded by the xBRCA1ΔC and xBARD1ΔC mutants lack residues 1355–1579 of *xBRCA1* and 647–772 of *xBARD1*, respectively (see supporting *Methods*). All mutations and cloning steps were validated by DNA sequencing of the resulting products.

Synthesis of mRNA for microinjections was carried out by using a Message Machine Kit (Ambion, Austin, TX) with *Not*I-linearized xBRCA1MpCS2, xBARD1MpCS2, or derivative plasmids as templates.

Antibodies. Rabbit polyclonal antisera were raised against GST fusion proteins, encoding residues 1001–1192 of xBRCA1 and 223–427 of xBARD1. The immune and preimmune sera (from the same animal) were affinity-purified by using the relevant peptide and an AminoLink kit (Pierce) according to the manufacturer's instructions. A rabbit polyclonal anti-hRad51 antibody (26) and the following mouse monoclonal Abs were used: anti-α-tubulin clone

Abbreviations: BRCA1, breast and ovarian cancer susceptibility protein 1; BARD1, BRCA1-associated RING domain protein; ODC, ornithine decarboxilase; MO, morpholino oligonucleotide; Msm, mismatches; IP, immunoprecipitation.

Data deposition: The sequences reported in this paper have been deposited in the GenBank database (accession nos. AF416868 and AF416869).

*Present address: Department of Radiation Oncology, Mayo Clinic, Rochester, MN 55905.

†J.B.A.G. and D.M.L. contributed equally to this work.

‡To whom reprint requests should be addressed. E-mail: david_livingston@dfci.harvard.edu.

The publication costs of this article were defrayed in part by page charge payment. This article must therefore be hereby marked "*advertisement*" in accordance with 18 U.S.C. §1734 solely to indicate this fact.

DM1A (Sigma), Anti-c-myc clone 9E10 (25), anti-HA-tag HA.11 (Covance, Richmond, CA), anti-green fluorescent protein (GFP) clone C163 (Zymed), and anti-Rad51 clone 3C10 (Upstate Biotechnology, Lake Placid, NY). Crossreactivity of two, different Rad51-specific Abs with xRad51 was verified by their ability to immunoprecipitate and to recognize in Western blot analysis an endogenous frog protein that comigrates with authentic human Rad 51 (*ca.* 37 kDa).

Cell Culture, RNA, and Protein Analysis. Transfections were carried out by using the standard calcium phosphate method. Analysis of RNA abundance was performed by Northern blotting of total RNA isolated from three *Xenopus* oocytes, eggs, or embryos, using the RNeasy Mini Kit (Qiagen). The specific ^{32}P-labeled DNA hybridization probes were: a 381-bp fragment of the *xODC* cDNA (27), the *Eco*RI/*Kpn*I fragment of the *xBRCA1*-A clone, and the *Eco*RI/*Xho*I fragment of the *xBARD1*-B clone. The latter two included nucleotides 3056–6177 and 715-2520 of full-length *xBRCA1* and *xBARD1* cDNAs, respectively.

Cells were lysed in a buffer containing 100 mM Hepes (pH 7.5), 200 mM NaCl, 40 mM EDTA, 4 mM EGTA, 100 mM NaF, 20 mM β-glycerophosphate, 2 mM sodium orthovanadate, 1% Nonidet P-40, and 1 tablet per 50 ml of the Complete Protease Inhibitor mixture (Boehringer Mannheim). For immunoprecipitations (IPs), extracts from 293 T cells or from 8–10 eggs or embryos were incubated with 1 μg of Ab on ice for 2–3 h, followed by incubation with 20 μl of protein A- or protein G-Sepharose beads (Amersham Pharmacia). HRP-protein A (Amersham Pharmacia; 1:2000) or HRP-goat anti-mouse Ig (Jackson ImmunoResearch; 1:10,000) were used for immunodetection of Western blots.

Embryos, RNA, and Oligonucleotide Microinjections. Adult *X. laevis* were obtained from NASCO (Ft. Atkinson, WI). Ovulation of females and fertilization of eggs was carried out as described (28). Embryos were cultivated in 0.1× Marc's Modified Ringers (MMR) and staged (29).

For microinjection experiments, mRNA and MOs were diluted in nuclease-free water. Two or four cell-stage embryos were suspended in 3% Ficoll in 0.5× MMR and injected four times in the marginal zone. MOs were obtained from GeneTools (Philomath, OR). The following antisense MOs were used: 5′-GGTCATTTTACTTTGTCCTGTCCCT-3′; 5′-CAACTTGCTCGCTGAGGGCACACAC-3′; and 5′-GTCCTGTCCCTTAAATGCAACTTG-3′ (xBRCA1 AS#1, xBRCA1 AS#2, and xBRCA1 AS#3, respectively) and 5′-CCTTAGCAGCATAATGAGGGGAGCC-3′ and 5′-CACTCCCGTTGATTAGACGTTCCGA-3′ (xBARD1 AS#1 and xBARD1 AS#2, respectively). The following control MOs were used: 5′-CCTCTTACCTCAGTTACAATTTATA-3′ (standard control oligo), 5′-GGTgATTaTACTTTGTCCaGTCgCT-3′ [(xBRCA1, 4-bp mismatch antisense MO #1, xBRCA1 mismatches (xBRCA1 Msm)], and 5′-CCTaAGCtGCATAATGAGcGGAcCC-3′ (xBARD1, 4-bp mismatch antisense MO #1, xBARD1 Msm). In general, the following embryo injection doses were used: 20–50 ng for xBRCA1 AS#1 and xBARD1 AS#1 and 40–80 ng for xBRCA1 AS#3 and xBARD1 AS#2.

Embryo Analysis. For histological examination, formaldehyde-fixed embryos were sectioned transversely (10 μm thickness) and stained (30). For mitotic index and karyotype analyses, tadpoles were suspended in 0.02% benzocaine in MMR and tails were excised. They were then incubated in distilled water for 20 min and squashed between a Superfrost slide and a coverslip in a drop of 70% acetic acid, using the Quick-Grip Bar Clamp. For karyotype analysis, this step was preceded by incubation of tail tips in 1% colchicine in Hanks' balanced salt solution for 2 h. The squashed tail preparations were incubated on dry ice for at least 10 min. The coverslip was quickly peeled off with a razor blade and the slide fixed in ethanol and stained with KaryoMax Giemsa Stain (GIBCO/BRL). The squashes were mounted in Permount (Fisher Scientific) and analyzed in a Nikon VFM microscope. The images were acquired digitally and processed with ADOBE PHOTOSHOP (Adobe Systems, Mountain View, CA). Nuclei were counted by using the public domain NIH IMAGE program (http://rsb.info.nih.gov/nih-image/). Genomic DNA was obtained from five stage-37 embryos, using the Puregene DNA Isolation kit (Gentra Systems). DNA abundance (μg per embryo) was calculated based on $A_{260\ nm}$ measurements.

Apoptotic cell death in embryos was measured by using the Cell Death Detection ELISA^{PLUS} system (Roche Molecular Biochemicals) according to the manufacturer's instructions.

Results

Conservation of BARD1 and BRCA1 Genes. We detected a large ORF in the *Arabidopsis thaliana* genome (composite of accession nos. PIR T04938 and PIR T10649). This region encodes a predicted protein with an N-terminal RING finger and a C-terminal BRCT domain that bears significant homology to the corresponding motifs of human BRCA1 and BARD1 (Fig. 1*A* and Fig. 6, which is published as supporting information on the PNAS web site). Certain residues within these *Arabidopsis* domains are conserved in both human proteins, suggesting that all three proteins share at least one common function. Other sequences of the *Arabidopsis* RING and BRCT motifs are uniquely shared with either BRCA1 or BARD1, but not both, implying that each also possesses individuated functions. These findings also suggest that yet other nonmammalian genomes encode BRCA1 and BARD1 orthologs.

To test this hypothesis, we searched for BRCA1- and BARD1-related sequences in *X. laevis*. By degenerate primer-directed PCR (see Fig. 6*B*) performed on *Xenopus* embryonic RNA with both *BRCA1*- and *BARD1*-related primers, specific cDNA products were generated. These structures were then used to isolate corresponding, full-length *BRCA1* and *BARD1* cDNAs from *Xenopus* cDNA libraries. The resulting, full-length *xBARD1* and *xBRCA1* cDNAs encode proteins of 772 and 1579 residues, respectively. Each is homologous to its human counterpart (Fig. 1*A*). Most of the residues common to human BARD1 and the *Arabidopsis* protein exist in frog BARD1. The same is true for BRCA1. Both proteins contain N-terminal RING finger and paired C-terminal BRCT repeats, and, like its human counterpart, xBARD1 contains three serial ankyrin repeats. The overall sequence identity between the human and frog BARD1 and BRCA1 homologs is 50% and 35%, respectively, with some local regions of much higher homology (Fig. 1*A*).

Certain cancer-predisposing, *BRCA1* missense mutations map to the RING finger. Others map to the BRCT region. Some of the wild-type (wt) BRCA1 residues targeted in these cases are triply conserved among the *Arabidopsis* protein and *Xenopus* and human BARD1 and BRCA1 (Fig. 6). This leads to speculation that there are elements of BRCA1 and BARD1 tumor suppression function that are contributed by ancient, highly conserved cell survival activity/activities. Moreover, the *Arabidopsis* RING finger is most similar to that of BRCA1, whereas its BRCT motifs most closely resemble those of BARD1 (Fig. 1*A*). Thus, the predicted *Arabidopsis* protein may be homologous to a common ancestor of vertebrate BARD1 and BRCA1.

Expression of the BARD1 and BRCA1 Genes in Frog Oocytes and Embryos. BRCA1 and BARD1 transcripts of 6.0 kb and 4.4 kb, respectively, were detected in *Xenopus* oocytes, eggs, and embryos, and were most abundant from the oocyte stage up to the onset of gastrulation (stage 10; Fig. 1*B*). Affinity-purified Ab to xBRCA1 and xBARD1, but not preimmune IgGs, recognized polypeptides of 210 kDa and 100 kDa, respectively, in egg and embryo extracts. The electrophoretic mobilities of these proteins were identical to those of clonal xBRCA1 and xBARD1.

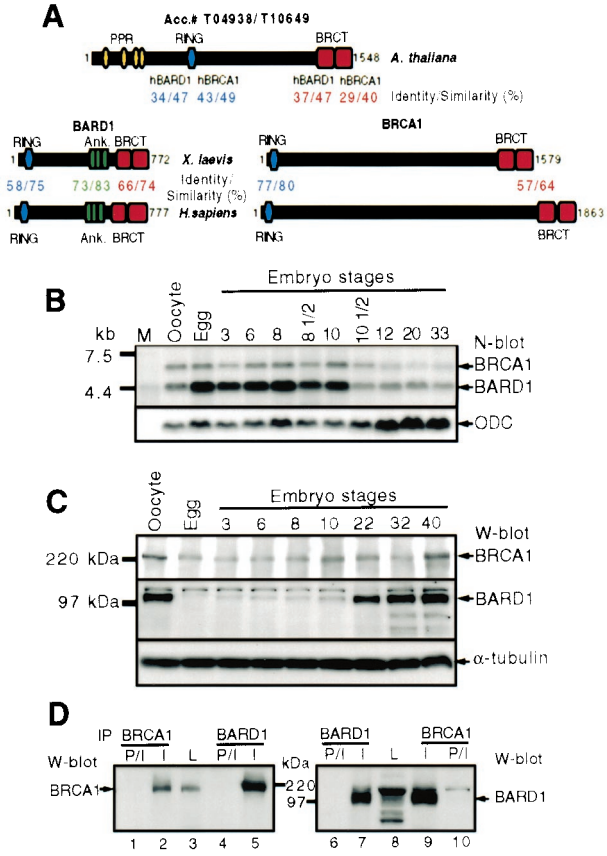

Fig. 1. BRCA1 and BARD1 Orthologs of *A. thaliana* and *X. laevis*. (*A*) Domain structure of frog and human BRCA1 and BARD1, and the putative *Arabidopsis* BRCA1/BARD1 ortholog. PPR, Pentatrico Peptide Repeat; RING, RING finger domain; Ank, Ankyrin repeat; BRCT, BRCA1 C- terminal motif. The first and the last residues of each protein are noted. The sequence identity/similarity between certain segments of human BRCA1 and BARD1 (the RING, ankyrin repeats, and 2xBRCT motifs) and their frog and *Arabidopsis* orthologs are indicated. (*B*) Electophoretically fractionated total RNA from embryos at the indicated stages was hybridized to specific, radioactively labeled *xBRCA1-*, *xBARD1-*, and *Xenopus* ornithine decarboxylase (*ODC*) probes. Bands were detected by autoradiography. mRNA transcripts and positions of RNA markers [the Radiolabeled RNA Ladder System (GIBCO), lane M] are indicated. (*C*) Total cell extracts of ten oocytes/eggs/embryos per sample were subjected to IP with xBRCA1- and the xBARD1-specific Abs. Immunoprecipitates were fractionated by SDS/PAGE and gels immunoblotted with xBRCA1- and xBARD1-specific Abs. Lysate from ½ of an embryo was immunoblotted with the α-tubulin Ab as a loading control. (*D*) BRCA1 and BARD1 complex formation in *Xenopus* embryos. Lysates of stage-12 embryos were IPd with xBRCA1- or xBARD1-specific immune (I) Ig, or preimmune (P/I) Ig. Lysates (L) and immunoprecipitates were analyzed by Western blotting using xBRCA1 (*Left*) or xBARD1 (*Right*) Ab. Combined lysates from two embryos were loaded in lanes 3 and 8. Precipitates from combined lysates of five embryos were loaded in lanes 1, 2, 6, and 7; precipitates from combined lysates of 20 embryos were loaded in lanes 4, 5, 9, and 10, respectively.

xBRCA1 Ab did not recognize xBARD1, and xBARD1 Ab did not recognize xBRCA1 (Figs. 1*C* and 5 and data not shown). There was a decline in BRCA1 and, especially, BARD1 abundance during oocyte maturation. However, at stage 10, both proteins began to accumulate. Thus, the relative abundance of BARD1 protein and its mRNA inversely correlated during early development (Fig. 1 *B* vs. *C*).

In *Xenopus* oocytes, eggs, and stage-12 embryos, most BRCA1 and BARD1 molecules were tightly complexed to one another (Fig. 1*D*). In addition, overexpression of either xBRCA1 or xBARD1 in cultured human cells led to the appearance of mixed *Xenopus*–human heterodimeric complexes (data not shown). Thus, there

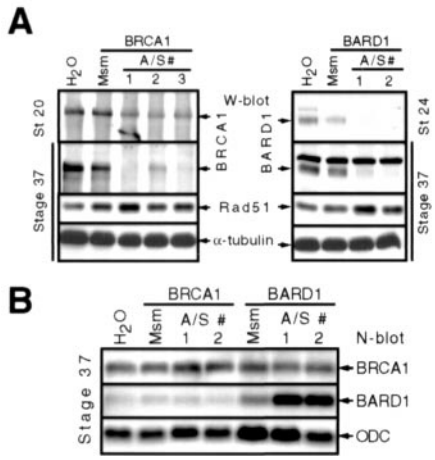

Fig. 2. Depletion of BRCA1 and BARD1 with specific antisense MOs. (*A*) Embryos were injected with 40 ng of alternative BRCA1-specific (BRCA1A/S #1, #2, and #3) or BARD1- specific (BARD1 A/S #1 and #2) antisense MOs. The control embryos were injected with water (H_2O) or with 40 ng of MOs that were each identical to the BRCA1- or BARD1-specific antisense MOs #1 but contained four dispersed nucleotide Msm. Lysates of the indicated embryos were analyzed by Western blotting with Rad51- and α-tubulin-specific Ab or by IP and Western blotting with xBRCA1- and xBARD1-specific Abs. (*B*) Total RNA from stage-37 embryos, which were treated as in *A*, was analyzed by Northern blot hybridization, as described for Fig. 1*B*.

appears to be a high degree of evolutionary conservation of the BRCA1 and BARD1 structures that support heterodimer formation, underscoring the likely importance of BRCA1/BARD1 heterodimerization in the tumor suppression process.

Specific Antisense Depletion of BRCA1 and BARD1 in Frog Embryos. Two-cell frog embryos were injected with specific BRCA1 or BARD1, morpholino antisense oligonucleotides (MOs) (31–33). In both cases, gradual depletion of the corresponding protein ensued (Fig. 2*A*). The direct effect of each antisense MO was likely specific to its cognate protein because, during cell-free synthesis, the BRCA1 antisense reagent interfered with BRCA1 mRNA translation and not with that of the BARD1 and *vice versa* (data not shown). Depletion began at the onset of gastrulation (stage 10), progressed to stage 20–24 (early tadpole, 2 days), and persisted to at least stage 42 (mature tadpole, *ca.* 3½ days). No significant depletion of α-tubulin or of the BRCA1-interacting protein, Rad51, was detected in these embryos. Neither BARD1 nor BRCA1 were significantly depleted when a scrambled MO or antisense MO containing four mismatches was injected (Fig. 2*A*).

No major drop in BARD1 or BRCA1 mRNA levels was observed in BARD1 or BRCA1 antisense MO-injected embryos (Fig. 2*B* and data not shown). Thus, the antisense effect on protein abundance was mediated posttranscriptionally. The BARD1 mRNA level actually rose in embryos injected with either of two different BARD1 antisense MOs (Fig. 2*B*). Given the inverse correlation between BARD1 mRNA and protein expression during early embryogenesis, it may be that BARD1 controls the abundance of its own mRNA by a negative feedback mechanism.

BARD1 or BRCA1 Deficiency Perturbs *Xenopus* Development. Antisense BRCA1- or BARD1-depleted embryos experienced gross phenotypic abnormalities. There were no overt defects in germ layer formation, gastrulation, or neurulation up to stage 20 in BRCA1-depleted embryos. After this stage, there was a progressive delay in development, as evidenced by the presence of a shortened axis and large quantities of unresorbed yolk. This was accompanied by axial defects, epidermal cysts, and malformations of the heart, large vessels, and gut (Fig. 3 *A* and *B*, Fig.

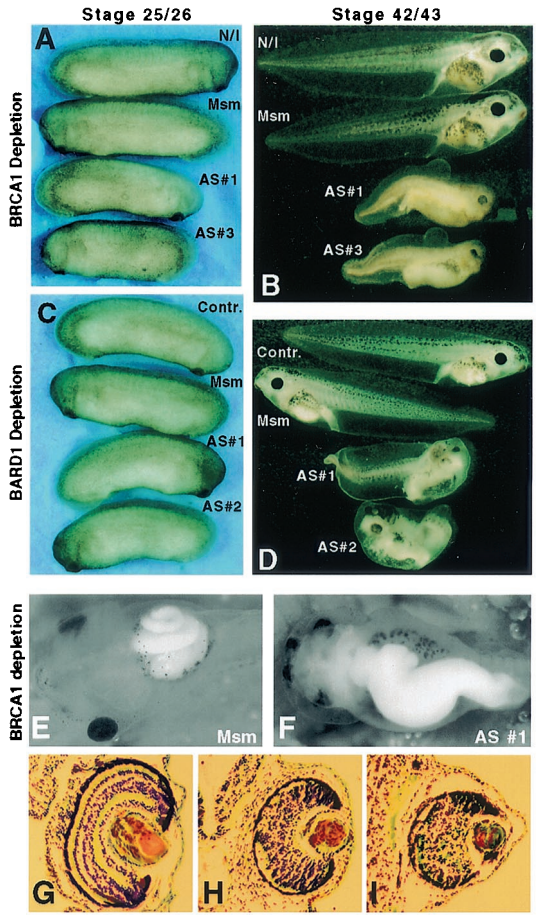

Fig. 3. BRCA1- and BARD1-depleted *Xenopus* embryos. (*A* and *B*) Embryos were either left uninjected (N/I) or injected with MOs: xBRCA1 Msm (30 ng), xBRCA1 AS#1 (30 ng), and xBRCA1 AS#3 (60 ng); (*C* and *D*) xBARD1 Msm (30 ng), xBARD1 AS#1 (30 ng), and xBARD1 AS#2 (70 ng) or with the control MO (Contr., 70 ng). Representative embryos at stages 25/26 (*Left*) and 42/43 (*Right*) are shown. Note the progressive phenotypic changes in the antisense-treated embryos. (*E* and *F*) The ventral view of representative stage-45 embryos, injected with 20 ng of the xBRCA1 Msm (*E*) or xBRCA1 AS#1 (*F*). Note the poor segregation of the alimentary canal and impaired coiling of the intestinal tube in the embryo even at this relatively low dose of antisense MO (*F*). Similar defects were observed in the BARD1-depleted embryos (data not shown). (*G–I*) The eye of a stage-42 embryo, injected with 25 ng of the BRCA1 Msm (*G*), xBRCA1 AS#1 (*H*), or xBARD1 AS#1 (*I*). Note the lack of retinal layers and the absence of degeneration of nuclei in the central lens fibers in the antisense MO-treated embryos (*H* and *I*). Similar defects were observed in embryos injected with xBRCA1 AS#3 and xBARD1 AS#2. The eye structures of the noninjected and the mismatch MO-injected embryos were histologically indistinguishable from one another (data not shown).

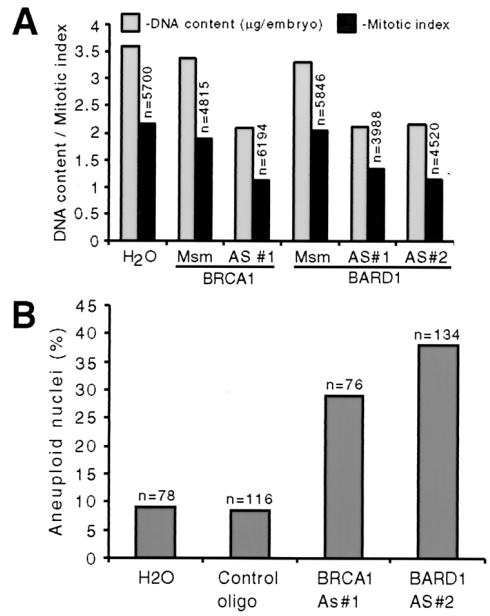

Fig. 4. Deficient proliferation and chromosomal instability in BRCA1- and BARD1-deficient embryos. (*A*) Embryos were injected with water or with 30 ng each of the MOs: xBRCA1 Msm, xBRCA1 AS#1, xBARD1 Msm, and xBARD1 AS#1, or with 60 ng of xBARD1 AS#2. The DNA content and the mitotic index were analyzed at stage 37. (*B*) Embryos were injected with xBRCA1 AS#1 (25 ng), xBARD1 AS#2 (60 ng), or a control oligonucleotide (60 ng). The chromosome number was analyzed in the stage-37–40 embryos. Aneuploid chromosome numbers ranged from 32 to 104 per cell in the antisense-treated embryos. A euploid, somatic *X. laevis* cell contains 36 chromosomes (38).

7 *B* and *C*, which is published as supporting information on the PNAS web site, and data not shown). The phenotype of BARD1-depleted embryos was similar, although less severe (Fig. 3 *C* and *D* and Fig. 7 *D* and *E*). Few or no abnormalities accompanied the injection of scrambled or mismatched derivatives of the wt MOs (Figs. 3 and 7). The phenotypes of BRCA1- and BARD1-depleted embryos were highly (>90%) penetrant.

Attempts to rescue these abnormalities by co-injection of the relevant mRNA met with success in some, but not all experiments, in keeping with the observation that injected BARD1 and BRCA1 mRNAs, although templates for specific protein synthesis, failed to permeate the entire embryo and were not efficiently translated, especially after stage 30 (note truncated BRCA1 products in lanes 3–5 of Fig. 5*B*; data not shown). Moreover, antisense MOs are exceedingly stable and persist through at least stage 45. However, the severity of the abnormal phenotype correlated with the degree of depletion of the target protein; the timing of phenotype development was constant among various batches of MO; and multiple BRCA1 and BARD1 antisense MOs produced related, albeit nonidentical phenotypes. Thus, these abnormalities are not likely to be nonspecific effects.

Most tissues in the affected embryos were present but disorganized (data not shown). The most obvious malformation occurred in the gut, where the alimentary canal either did not form (at higher doses of antisense MO) or, when it did form, neither segregated nor coiled (at lower doses of MO; Fig. 3 *E* and *F* and Fig. 7 *B–E*). Neuroepithelium was also severely affected in both BRCA1- and BARD1-depleted embryos, as shown by the presence of a malformed neural tube and eye structures (compare Fig. 3 *G* with *H* and *I*). Not surprisingly, both BRCA1 and BARD1 antisense-treated embryos were nonviable.

By stage 37, both BARD1- and BRCA1-antisense MO-injected embryos contained 40–42% less DNA than controls, and the mitotic index was depressed (Fig. 4*A*). No increase in apoptotic activity was detected in either set of embryos (data not shown). Thus, the decrease in DNA content is likely a result of deficient proliferation and not increased apoptosis. Aneuploidy was observed in 29–38% of mitotic cells in BRCA1- and BARD1-depleted embryos, respectively, compared with 8.6% in controls (Fig. 4*B*).

Mutual Abundance Control of BRCA1 and BARD1. Antisense depletion of BRCA1 was generally accompanied by a sustained decrease in BARD1 abundance (Fig. 5*A Left*). Injection of BRCA1 mRNA into unperturbed or BRCA1 antisense MO-treated embryos led to an accumulation of BARD1 above the level in control embryos (Fig. 5*B* and data not shown). In addition, BARD1 was readily overproduced in unperturbed,

CELL BIOLOGY

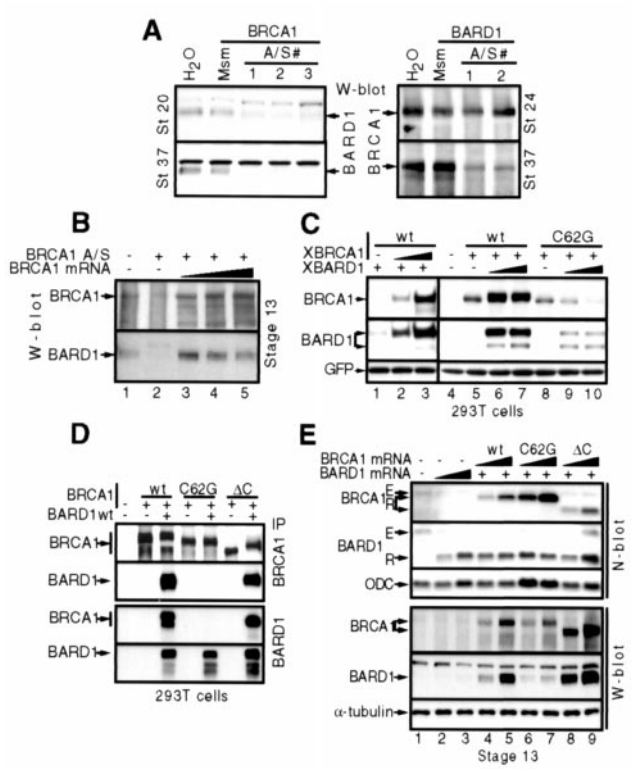

Fig. 5. Reciprocal control of BRCA1 and BARD1 abundance. (*A*) Cell lysates from the MO-treated embryos were analyzed by standardized Western blotting for BARD1 and BRCA1 abundance, respectively, at the indicated stages. Identical samples of embryo cell lysates were analyzed in this experiment and in the experiment described in Fig. 2*A*. (*B*) BRCA1 and BARD1 protein in stage 13 embryos that had been injected with 40 ng of xBRCA1 AS#1 alone (lane 2) or coinjected with this reagent and with 200, 400, or 600 pg of xBRCA1 mRNA (lanes 3, 4, and 5, respectively). (*C*) 293 T cells were transfected with 3 μg of xBARD1 wt cDNA expression vector, alone (lane 1) or together with 3 μg or 9 μg of xBRCA1 wt cDNA expression vector (lanes 2 and 3, respectively), or with 3 μg of xBRCA1 wt cDNA (lane 5) or xBRCA1 C62G cDNA expression vector (lane 8), alone or together with 3 μg (lanes 6 and 9) or 9 μg (lanes 7 and 10) of xBARD1wt cDNA expression vector. The transfection mixtures each contained 5% of green fluorescent protein (GFP) cDNA, cloned in an expression vector. Each lane was analyzed by Western blotting with the indicated Ab. Anti-GFP Ab was used to detect GFP abundance in each lane. (*D*) 293 T cells were transfected with the indicated xBRCA1 cDNA expression vector, alone or together with the wt xBARD1 cDNA vector. The cell lysates were subjected to IP with the xBRCA1- or xBARD1-specific Ab (*Upper* and *Lower*, respectively), and each immunoprecipitate was immunoblotted with both of these Ab. (*E*) *Xenopus* embryos were injected with 300 and 600 pg of xBARD1 mRNA (lanes 2 and 3, respectively) or were coinjected with 300 pg of xBARD1 mRNA and 300 pg (lanes 4, 6, and 8) or 600 pg (lanes 5, 7, and 9) of the indicated xBRCA1 mRNA. At embryo-stage 13, total RNA was isolated from half of each injected embryo set and analyzed by Northern blot hybridization as described for Fig. 1*B* (*Upper*). The endogenous (E) and the recombinant (R) forms of the xBRCA1 and xBARD1 mRNAs are indicated by arrows. In extracts of the other half of each experimental embryo set, the abundance of xBRCA1 and xBARD1 were analyzed by IP/Western blotting as in Fig. 2*A* (*Lower*). α-tubulin was detected by direct Western blotting.

stage-13–15 embryos when its mRNA was co-injected with BRCA1 mRNA, but not when injected alone (Fig. 5*E*, lanes 2–5). No effect of BRCA1 mRNA on the level of endogenous BARD1 mRNA was observed (Fig. 5*E Upper*). Thus, BRCA1 positively regulates and is limiting for BARD1 abundance in the early stage embryo, and the effect is not a result of enhanced BARD1 mRNA synthesis or stability.

Antisense BARD1 depletion did not affect BRCA1 abundance through stage 24 (Fig. 5*A Right Upper*). Moreover, following BRCA1 mRNA injection during this period, the level of BRCA1 expression was proportional to the quantity of BRCA1 mRNA injected and was unaffected by BARD1 coexpression (Fig. 5*B* and data not shown). However, by stage 37 a dramatic decrease in BRCA1 abundance was detected in BARD1-depleted embryos without a change in BRCA1 mRNA (Fig. 5*A Right Lower* and Fig. 2*B*). Thus, relatively late in development BARD1 acquires the ability to regulate BRCA1 abundance. Notably, BRCA1 depletion was still associated with a fall in BARD1 abundance in these later-stage embryos. Thus, by stage 37 each protein affects the abundance of the other, again without affecting mRNA synthesis or stability.

Reciprocal regulation of BRCA1 and BARD1 abundance also occurs in cultured human cells (293 T). Specifically, endogenous BRCA1 levels were artificially elevated by transiently transfecting a frog or human BARD1 expression vector, and *vice versa* (Fig. 5*C*, lanes 1–7). Moreover, pulse–chase analysis of BRCA1 and BARD1 turnover in human cells indicated that ectopic overproduction of human BARD1 led to overt stabilization of human BRCA1. A less dramatic but analogous effect of BRCA1 was observed on BARD1 (Fig. 8*A*, which is published as supporting information on the PNAS web site). Similar results were observed with the *Xenopus* proteins analyzed in 293 T cells (data not shown).

Heterodimerization Is Necessary for BRCA1/BARD1 Abundance Control. An xBRCA1 cysteine residue (C62), located in the relevant RING finger domain, corresponds to C61 of hBRCA1 (Fig. 6*A*), the site of a clinically relevant C → G mutation that also eliminates BRCA1/BARD1 complex formation (2). It was replaced by Gly to generate xBRCA1 C62G. This mutation abolished xBRCA1/xBARD1 complex formation, as expected. It also nullified the ability of xBRCA1 to increase xBARD1 levels in embryos (Fig. 5 *D* and *E*). It also prevented bidirectional xBRCA1 ↔ xBARD1 stabilization in cultured cells (Fig. 5*C*, lanes 8–10). A similar C → G mutation was created in the corresponding cysteine (C77) of the xBARD1 RING. Surprisingly, it failed to abolish the xBARD1/xBRCA1 interaction, nor did it perturb mutual abundance control in *Xenopus* embryos or human cultured cells (Fig. 8 *B* and *C* and data not shown). C-terminal truncation mutants of either BRCA1 or BARD1, lacking their BRCT motifs, also heterodimerized and underwent mutual abundance control (Fig. 5 *D* and *E*, Fig. 8 *B* and *C*, and data not shown). Thus, among a number of mutations in conserved domains, only that which prevented heterodimerization interfered with BARD1/BRCA1 abundance control.

Discussion

xBRCA1 and xBARD1 are functional homologs of their mammalian counterparts. They heterodimerize in a xBRCA1 RING-dependent manner, just as in mammals (2). Moreover, as in mice, loss of xBRCA1 expression during embryogenesis is a lethal event. The same is true for BARD1, indicating that both proteins play vital roles in *Xenopus* embryogenesis.

BARD1- and BRCA1-depleted embryos experienced related phenotypes, marked by retarded development, multiple organ dysgenesis, and defects in certain discrete mesenchymal and epithelial (e.g., endodermal) structures. Thus, it seems likely that BRCA1 and BARD1 share common functions during frog development. Notably, endodermal differentiation occurs relatively late in *Xenopus* development, an observation that, despite injection of the relevant antisense MOs at the two-cell stage, is matched by the relatively late onset of BARD1 and BRCA1 depletion in this organism.

Epithelial abnormalities are not new to BRCA1-depleted organisms. Certain BRCA1−/− mouse embryos revealed dramatic neuroepithelial abnormalities (34). Defects in breast ductal development were noted after breast-specific BRCA1 elimination (35). Moreover, tumors arising in BRCA1+/− patients are largely

epithelial (breast and ovarian carcinomas); so are tumors bearing biallelic BARD1 genetic defects (breast, ovarian, and uterine carcinomas; ref. 18), possibly reflecting not only the close functional interplay between BRCA1 and BARD1, but also their joint participation in certain epithelial differentiation events.

BRCA1 or BARD1 depletion led to aneuploidy, in keeping with the evidence that BRCA1 and, likely, BARD1/BRCA1 heterodimers contribute to genome stability control (6, 7). Moreover, as in the mouse, the xBARD1- and xBRCA1 depletion-dependent defect in cell proliferation might, at least in part, reflect widespread checkpoint activation (3, 6, 7).

The similarity of the BARD1- and BRCA1-depletion phenotypes may also reflect a significant degree of interconnection of the biochemical functions of the two proteins. In this regard, BARD1 depletion was accompanied by BRCA1 depletion and *vice versa*. The mechanism appears to be a product of loss of heterodimerization-dependent BRCA1 and BARD1 stability control.

In this regard, the *Xenopus* equivalent of a disease-producing BRCA1 RING domain mutant was defective in heterodimerizing with stabilizing BARD1, suggesting that mutual abundance control depends on efficient heterodimer formation and is potentially a significant contributor to BRCA1 tumor suppression function. In such a setting, one might envision BARD1 contributing to the maintenance of sufficient levels of intact BRCA1 needed to maintain a state of active tumor suppression.

BARD1 likely has breast and ovarian tumor suppressing properties in its own right (17, 18). Therefore, a BRCA1 RING mutation may have another effect—i.e., on the maintenance of sufficient levels of another tumor suppressing protein, such as BARD1. A fall in BARD1 level may, in turn, lead to BRCA1 instability, creating a vicious cycle with respect to the maintenance of BRCA1 + BARD1 tumor suppression function.

Both RING domain proteins exhibit E3 ubiquitin ligase function *in vitro*, and the specific activity of the heterodimer is considerably greater than that of either partner alone (21). Because mutual abundance control appears to be a proteasome-mediated process, one wonders about a link between the potential E3 activity of the heterodimer and BARD1/BRCA1 abundance control. It seems unlikely, however, that heterodimerization is accompanied by reciprocal polyubiquitination of BARD1 and BRCA1, for this would be expected to destabilize the two proteins.

Moreover, heterodimers in which the BARD1 RING was mutated were active in mutual abundance control, implying that the two RING domains do not function in parallel in this process.

Stabilization of one RING domain protein by another has been observed previously: the oncoprotein MDM2 and a closely related protein, MDMX, interact through their RING finger regions, and this interaction protects the former from degradation (36, 37).

Much remains to be learned of how BRCA1 and BARD1 deliver their breast and ovarian tumor suppressing signals. In this regard, the discovery of plant and frog orthologs of these proteins and the knowledge that the functions of the frog proteins resemble, at least in part, those of their human and mouse counterparts, imply that their tumor suppression functions are likely derived from one or more of their well conserved cell and organ survival functions. The frog system represents an opportunity to explore biochemical aspects of these relationships.

We thank Isabel M. Dominguez, Thomas J. McGarry, Yosef Landesman, and Olga Ossipova for support and advice, Paul Morcos and Janet Heasman for sharing their expertise in the use of antisense MOs, Ralph Scully, Ramesh A. Shivdasani, and Ronny Drapkin for many helpful discussions, Ralph Scully for certain plasmids and the Rad51 Ab, Douglas W. DeSimone for the cDNA library, and Anton Chestukhin and Larisa Litovchick for valuable suggestions concerning the cycloheximide chase experiments. This work was funded by the National Cancer Institute. V.J. was supported by a Human Frontier Science Program (HFSP) Fellowship and by a Massachusetts Department of Public Health Breast Cancer Research Grant. I.B.A.G. was supported by grants from the National Institute of Child Health and Human Development and the National Science Foundation.

1. Miki, Y., Swensen, J., Shattuck-Eidens, D., Futreal, P. A., Harshman, K., Tavtigian, S., Liu, Q., Cochran, C., Bennett, L. M. & Ding, W. (1994) *Science* **266,** 66–71.
2. Wu, L. C., Wang, Z. W., Tsan, J. T., Spillman, M. A., Phung, A., Xu, X. L., Yang, M. C., Hwang, L. Y., Bowcock, A. M. & Baer, R. (1996) *Nat. Genet.* **14,** 430–440.
3. Hakem, R., de la Pompa, J. L., Sirard, C., Mo, R., Woo, M., Hakem, A., Wakeham, A., Potter, J., Reitmair, A., Billia, F., Firpo, E., Hui, C. C., Roberts, J., Rossant, J. & Mak, T. W. (1996) *Cell* **85,** 1009–1023.
4. Liu, C. Y., Flesken-Nikitin, A., Li, S., Zeng, Y. & Lee, W. H. (1996) *Genes Dev.* **10,** 1835–1843.
5. Ludwig, T., Chapman, D. L., Papaioannou, V. E. & Efstratiadis, A. (1997) *Genes Dev.* **11,** 1226–1241.
6. Shen, S. X., Weaver, Z., Xu, X., Li, C., Weinstein, M., Chen, L., Guan, X. Y., Ried, T. & Deng, C. X. (1998) *Oncogene* **17,** 3115–3124.
7. Xu, X., Weaver, Z., Linke, S. P., Li, C., Gotay, J., Wang, X. W., Harris, C. C., Ried, T. & Deng, C. X. (1999) *Mol. Cell.* **3,** 389–395.
8. Scully, R., Chen, J., Plug, A., Xiao, Y., Weaver, D., Feunteun, J., Ashley, T. & Livingston, D. M. (1997) *Cell* **88,** 265–275.
9. Chen, J., Silver, D. P., Walpita, D., Cantor, S. B., Gazdar, A. F., Tomlinson, G., Couch, F. J., Weber, B. L., Ashley, T., Livingston, D. M. & Scully, R. (1998) *Mol. Cell* **2,** 317–328.
10. Wang, Y., Cortez, D., Yazdi, P., Neff, N., Elledge, S. J. & Qin, J. (2000) *Genes Dev.* **14,** 927–939.
11. Zhong, Q., Chen, C. F., Li, S., Chen, Y., Wang, C. C., Xiao, J., Chen, P. L., Sharp, Z. D. & Lee, W. H. (1999) *Science* **285,** 747–750.
12. Cantor, S. B., Bell, D. W., Ganesan, S., Kass, E. M., Drapkin, R., Grossman, S., Wahrer, D. C. R., Sgroi, D. C., Lane, W. S., Haber, D. A. & Livingston, D. M. (2001) *Cell* **105,** 149–160.
13. Moynahan, M. E., Chiu, J. W., Koller, B. H. & Jasin, M. (1999) *Mol. Cell* **4,** 511–518.
14. Gowen, L. C., Avrutskaya, A. V., Latour, A. M., Koller, B. H. & Leadon, S. A. (1998) *Science* **281,** 1009–1012.
15. Scully, R., Ganesan, S., Vlasakova, K., Chen, J., Socolovsky, M. & Livingston, D. M. (1999) *Mol. Cell* **4,** 1093–1099.
16. Snouwaert, J. N., Gowen, L. C., Latour, A. M., Mohn, A. R., Xiao, A., DiBiase, L. & Koller, B. H. (1999) *Oncogene* **18,** 7900–7907.
17. Irminger-Finger, I., Soriano, J. V., Vaudan, G., Montesano, R. & Sappino, A. P. (1998) *J. Cell Biol.* **143,** 1329–1339.
18. Thai, T. H., Du, F., Tsan, J. T., Jin, Y., Phung, A., Spillman, M. A., Massa, H. F., Muller, C. Y., Ashfaq, R., Mathis, J. M., *et al.* (1998) *Hum. Mol. Genet.* **7,** 195–202.
19. Kleiman, F. E. & Manley, J. L. (1999) *Science* **285,** 1576–1579.
20. Kleiman, F. E. & Manley, J. L. (2001) *Cell* **104,** 743–753.
21. Hashizume, R., Fukuda, M., Maeda, I., Nishikawa, H., Oyake, D., Yabuki, Y., Ogata, H. & Ohta, T. (2001) *J. Biol. Chem.* **276,** 14537–14540.
22. Lorick, K. L., Jensen, J. P., Fang, S., Ong, A. M., Hatakeyama, S. & Weissman, A. M. (1999) *Proc. Natl. Acad. Sci. USA* **96,** 11364–11349.
23. Ruffner, H., Joazeiro, C. A., Hemmati, D., Hunter, T. & Verma, I. M. (2001) *Proc. Natl. Acad. Sci. USA* **98,** 5134–5139.
24. Rupp, R. A., Snider, L. & Weintraub, H. (1994) *Genes Dev.* **8,** 1311–1323.
25. Evan, G. I., Lewis, G. K., Ramsay, G. & Bishop, J. M. (1985) *Mol. Cell. Biol.* **5,** 3610–3616.
26. Scully, R., Chen, J., Ochs, R. L., Keegan, K., Hoekstra, M., Feunteun, J. & Livingston, D. M. (1997) *Cell* **90,** 425–435.
27. Isaacs, H. V., Tannahill, D. & Slack, J. M. (1992) *Development (Cambridge, U.K.)* **114,** 711–720.
28. Sive, H. L., Grainger, R. M. & Harland, R. M. (2000) *Early Development of Xenopus laevis* (Cold Spring Harbor Lab. Press, Plainview, NY).
29. Nieuwkoop, P. D. & Faber, J., eds. (1994) *Normal Table of Xenopus laevis (Daudin)* (Garland Publishing, New York), 2nd Ed.
30. Cooke, J. (1979) *J. Embryol. Exp. Morphol.* **51,** 165–182.
31. Heasman, J., Kofron, M. & Wylie, C. (2000) *Dev. Biol.* **222,** 124–134.
32. Nasevicius, A. & Ekker, S. C. (2000) *Nat. Genet.* **26,** 216–220.
33. Summerton, J. (1999) *Biochim. Biophys. Acta* **1489,** 141–158.
34. Gowen, L. C., Johnson, B. L., Latour, A. M., Sulik, K. K. & Koller, B. H. (1996) *Nat. Genet.* **12,** 191–194.
35. Xu, X., Wagner, K. U., Larson, D., Weaver, Z., Li, C., Ried, T., Hennighausen, L., Wynshaw-Boris, A. & Deng, C. X. (1999) *Nat. Genet.* **22,** 37–43.
36. Sharp, D. A., Kratowicz, S. A., Sank, M. J. & George, D. L. (1999) *J. Biol. Chem.* **274,** 38189–38196.
37. Tanimura, S., Ohtsuka, S., Mitsui, K., Shirouzu, K., Yoshimura, A. & Ohtsubo, M. (1999) *FEBS Lett.* **447,** 5–9.
38. Graf, J. D. & Kobel, H. R. (1991) *Methods Cell Biol.* **36,** 19–34.